The Astrophysical Journal, 1000:155 (7pp), 2026 April 1 https://doi.org/10.3847/1538-4357/ae486a
© 2026. The Author(s). Published by the American Astronomical Society.
OPEN ACCESS

The FAST Galactic Plane Pulsar Snapshot Survey. IX. Timing Three Binary Pulsars with Wide Orbits and Low Orbital Eccentricities

Z. L. Yang[1,2], J. L. Han[1,2,3], W. Q. Su[1,2], C. Wang[1,2,3], J. P. Yuan[3,4], T. Wang[1], Yi Yan[1,2], J. Xu[1,3], W. C. Jing[1,2], P. F. Wang[1,2,3], N. N. Cai[1], D. J. Zhou[1], X. J. Chen[4], and D. Zhao[4]
[1] National Astronomical Observatories, Chinese Academy of Sciences, Jia-20 Datun Road, ChaoYang District, Beijing 100012, People's Republic of China; hjl@nao.cas.cn
[2] School of Astronomy and Space Science, University of Chinese Academy of Sciences, Beijing 100049, People's Republic of China
[3] State Key Laboratory of Radio Astronomy and Technology, Beijing 100101, People's Republic of China
[4] Xinjiang Astronomical Observatory, Chinese Academy of Sciences, Urumqi 830011, People's Republic of China
Received 2025 October 3; revised 2026 February 16; accepted 2026 February 18; published 2026 March 20

Abstract

Current pulsar timing models face challenges when applied to binary pulsars with wide orbits and low orbital eccentricities. The conventional Damour–Deruelle (DD) model accurately characterizes the orbits of such systems, but it suffers from strong correlations between the time of periastron passage (T_0) and the longitude of periastron (ω). The ELL1 model avoids these parameter correlations, yet fails due to the limitations of its first-order low-eccentricity approximation. Recent enhancements to the ELL1 model (dubbed ELL1+ model) have incorporated higher-order terms but retain the low-eccentricity approximation. In this study, we propose a further improved model, ELL1R, which eliminates reliance on the low-eccentricity approximation through rigorous calculation of the Römer delay. This modification can avoid strong parameter correlations in the DD model, and it can be used in systems with mild eccentricity, $0.01 \lesssim e \lesssim 0.1$, where the ELL1+ model cannot be used. Using the ELL1R model, we present the first phase-coherent timing solutions for three binary pulsars: PSR J1851–0108 (orbital period: 228 days), PSR J1910+0423 (886 days), and PSR J1923+2022 (777 days). Validation against the DD and ELL1+ models confirms that ELL1R yields consistent timing results while integrating the advantages of the two models. Our analysis further indicates that all three pulsars are mildly recycled. The companions of PSRs J1910+0423 and J1923+2022 are likely white dwarfs, whereas the nature of PSR J1851–0108's companion remains unknown.

Unified Astronomy Thesaurus concepts: Binary pulsars (153); Radio pulsars (1353); Pulsar timing method (1305)

1. Introduction

Binary pulsars have various types of companions with very different orbital parameters. Pulsar–white dwarf systems have small orbital eccentricities, and their orbital periods can be as long as about 1000 days (R. N. Manchester et al. 2005). These binary systems allow us to constrain violations of the strong equivalence principle and momentum conservation as well as Lorentz invariance (T. Damour & G. Schaefer 1991; C. M. Will 1993; N. Wex 1997, 2000). Parameters of pulsar timing solutions contain important information on locations, rotational slowdown, binary orbits, and relativistic effects. By comparing the predictions of the timing solutions with the measured times of arrival (TOAs) of pulses, the values and uncertainties of these parameters can be obtained.

Many timing models have been developed for binary pulsar timing, and selecting an appropriate model is essential for achieving a reliable phase-connected timing solution. The Blandford–Teukolsky (BT) model (R. Blandford & S. A. Teukolsky 1976) was proposed for the timing of the first known binary pulsar, PSR B1913+16 (R. A. Hulse & J. H. Taylor 1975). Later, T. Damour & N. Deruelle (1985, 1986) developed the Damour–Deruelle (DD) model, which provides a better description of relativistic effects, and nowadays the DD model is widely employed for binary pulsars with significant orbital eccentricities, such as double neutron star systems. However, for binary pulsars with low eccentricity ($e \ll 1$), the parameters ω (the longitude of periastron) and T_0 (the time of periastron passage) exhibit strong covariance. When fitting the orbital eccentricity e in such systems, timing software may terminate due to $e < 0$, complicating the search for a phase-connected solution.

For low-eccentricity binary pulsars, such as many pulsar–white dwarf systems, C. Lange et al. (2001) introduced the ELL1 timing model, in which ω, T_0, and e are replaced by the time of ascending node passage $T_{\rm asc} \equiv T_0 - (\omega/2\pi)P_{\rm orb}$ and two Laplace parameters $\epsilon_1 \equiv e\sin\omega$ and $\epsilon_2 \equiv e\cos\omega$. The Römer delay $\Delta_{\rm RB}$, which describes the variation in light travel time caused by orbital motion, is computed only to first order in the orbital eccentricity e (C. Lange et al. 2001). This approximation holds when $xe^2/c \lesssim \sigma_{\rm TOA}/N_{\rm TOA}^{1/2}$, where x is the projected semimajor axis, c is the speed of light, $\sigma_{\rm TOA}$ is the uncertainty of individual TOA measurements, and $N_{\rm TOA}$ is the number of TOAs. However, in many wide-orbit pulsar–white dwarf binary systems, xe^2 can reach values $\gtrsim$1 ms, and the accuracy of the first-order approximation is not enough.

Subsequent improvements were introduced by W. W. Zhu et al. (2019), who derived second-order eccentricity terms, and later by W. Fiore et al. (2023), who extended the calculation to third order. This enhanced version, referred to hereafter as the ELL1+ model, has been implemented in the TEMPO[5] software (including terms up to xe^2; D. Nice et al. 2015) and the PINT pulsar timing package (up to xe^3; J. Luo et al. 2021), though it remains unavailable in the widely used TEMPO2 software (G. B. Hobbs et al. 2006).

[5] http://tempo.sourceforge.net/

Original content from this work may be used under the terms of the Creative Commons Attribution 4.0 licence. Any further distribution of this work must maintain attribution to the author(s) and the title of the work, journal citation and DOI.

Table 1
FAST Observation Sessions for the Three Pulsars

PSR	J1851–0108	J1910+0423	J1923+2022
Observation MJD range	59480–61005	59768–61014	59180–60999
Total sessions	28	21	33
FAST GPPS (PI: J. L. Han)	4	9	6
PT2022_0047 (PI: W. Q. Su)	17	0	14
PT2023_0017 (PI: C. Wang)	0	0	3
PT2023_0102 (PI: W. Q. Su)	0	1	0
PT2023_0162 (PI: W. Q. Su)	2	3	1
PT2024_0089 (PI: Y. Yan)	0	2	0
PT2024_0173 (PI: J. Xu)	0	0	1
PT2024_0195 (PI: C. Wang)	0	0	1
PT2024_0199 (PI: W. Q. Su)	3	3	1
PT2024_0235 (PI: W. C. Jing)	1	0	0
ZD2025_6 (PI: J. P. Yuan)	0	2	6
PT2025_0211 (PI: T. Wang)	0	1	0
PT2025_0221 (PI: W. Q. Su)	1	0	0

In this paper, we present a refined timing model (hereafter referred to as the `ELL1R` model;[6] Z. L. Yang 2025) written in TEMPO2 format (G. B. Hobbs et al. 2006), which computes the Römer delay without relying on low-eccentricity approximations. We then applied it to three binary systems, PSRs J1851–0108, J1910+0423, and J1923+2022, which were discovered by the Five-hundred-meter Aperture Spherical radio Telescope (FAST; R. Nan 2006) during the Galactic Plane Pulsar Snapshot (GPPS) survey (J. L. Han et al. 2021, 2025). The initial orbital parameters of PSRs J1910+0423 and J1923+2022 have been published in P. F. Wang et al. (2025), and they are in orbits with long orbital periods of a few hundred days. PSRs J1910+0423 and J1923+2022 have very small orbital eccentricities $e < 0.01$, while PSR J1851–0108 has a mild orbital eccentricity in the range $0.01 \lesssim e \lesssim 0.1$. We obtained their new timing solutions accurately. In Section 2, FAST observations, the timing procedure, and our new timing model are introduced. In Section 3, we present the timing results of PSRs J1851–0108, J1910+0423, and J1923+2022 by using different timing models and discuss the pulsar properties and their possible origins. A summary of our work is presented in Section 4.

2. Observations and Data Reduction

2.1. FAST Observations

The three pulsars, PSRs J1851–0108, J1910+0423, and J1923+2022, were discovered in the FAST GPPS survey (J. L. Han et al. 2021, 2025). PSR J1851–0108 was discovered in a 21 minute snapshot observation on 2021 September 23 and later confirmed by a 15 minute tracking observation on 2021 October 5. PSR J1910+0423 was discovered in a 21 minute snapshot observation on 2022 July 9 and later confirmed by a 5 minute tracking observation on 2022 July 22. PSR J1923+2022 was discovered in a 15 minute tracking observation on 2020 November 27 and later confirmed by another 15 minute tracking observation on 2021 January 27. Their binary characteristics have been identified using changes of their barycentric spin periods (P. F. Wang et al. 2025).

In this work, we used all available FAST observations from the FAST GPPS survey and other FAST projects (see Table 1). The *L*-band 19-beam receiver has been used for all FAST observations, which covers the frequency range of 1.0–1.5 GHz. Data were recorded in the search mode with 4096 or 2048 frequency channels, with a sampling time of 49.152 μs. In most observations, the data from four polarization channels from the linear polarization feed, *XX*, *YY*, Re[X^*Y], and Im[X^*Y], were recorded. The polarization data were calibrated by using the periodic calibration noise signals injected for 120 s (for 10 minutes or longer sessions) or 40 s (for other sessions) at the beginning or the end of each observation session.

2.2. Pulsar Timing Procedure and `ELL1R` Timing Model

The orbital motion of a binary pulsar gives rise to variations in its line-of-sight velocity, which in turn cause changes in the observed barycentric spin period. These variations are described by a set of Keplerian orbital parameters: the orbital period $P_{\rm orb}$, the time of periastron passage T_0, the longitude of periastron ω, the projected semimajor axis x, and the orbital eccentricity e. For each observation session, we derived the barycentric spin period $P_{\rm bary}$ and the barycentric epoch $T_{\rm bary}$ using the `prepfold` command in PRESTO, a software package designed for pulsar data analysis (S. M. Ransom 2001). Adopting the approach of B. Bhattacharyya & R. Nityananda (2008), we then performed a two- or four-dimensional search over orbital parameters to fit the barycentric periods measured at different epochs.

Using these initial orbital parameters, we folded the observational data into pulse profiles using DSPSR (W. van Straten & M. Bailes 2011). Radio frequency interference (RFI) was automatically removed using the method described in X. Chen et al. (2023), and polarization profiles were derived following the procedure in P. F. Wang et al. (2023). TOAs were extracted from the resulting profiles using the PSRCHIVE software suite through the following steps: (1) manual verification of RFI excision using `psrzap`; (2) compressing each session's data into one polarization channel (total intensity), two subintegrations, and four subbands using the `pam` command (A. W. Hotan et al. 2004); and (3) extracting TOAs via the `pat` command by cross correlating the profiles with a one-dimensional frequency-averaged template generated by `paas` (A. W. Hotan et al. 2004).

[6] Available at https://github.com/Zony-naoc/ELL1Rmodel

The TOAs were analyzed using the high-precision pulsar timing package TEMPO2 (G. B. Hobbs et al. 2006). The ELL1 timing model is commonly used for binary systems with low orbital eccentricity. In this model, the Römer delay $\Delta_{\rm RB}$ is given by (C. Lange et al. 2001)

$$\Delta_{\rm RB} \approx x\left[\sin\Phi + \frac{\epsilon_1}{2}\sin(2\Phi) - \frac{\epsilon_2}{2}\cos(2\Phi)\right], \quad (1)$$

where Φ is the orbital phase. It is worth noting that, in addition to terms of order xe^2, the ELL1 model also omits the term $xe\sin\omega \equiv x\epsilon_1$ in the Römer delay expression (A. Susobhanan et al. 2018). If $x\epsilon_1$ varies with time, this omission can introduce a small systematic bias in the measured spin period. For the wide-orbit systems PSRs J1851–0108, J1910+0423, and J1923+2022, whose xe^2/c are 3.7, 1.4 $\times$ 10^{-3}, and 1.1 $\times$ 10^{-4} s, respectively, the original ELL1 model implemented in TEMPO2 is not well suited for their timing since the low-eccentricity approximation $xe^2 \lesssim \sigma_{\rm TOA}/N_{\rm TOA}^{1/2}$ is no longer true. The ELL1+ model can be used for timing PSRs J1910+0423 and J1923+2022, but it remains unsuitable for PSR J1851–0108 due to its large $xe^4/c = 0.065$ s. Note that the ELL1+ model is not currently included in the standard TEMPO2 distribution (G. B. Hobbs et al. 2006).

Although the BT and DD models can accurately calculate the Römer delay, they are not suitable for systems with low orbital eccentricities. Traditionally, the last digit of a measured value is uncertain and should align with the place of the uncertainty. In the BT or DD model, the high covariance between ω and T_0 significantly increases their uncertainties. Therefore, if the BT or DD model was applied for these systems, the reported values of ω and T_0 cannot accurately reproduce the timing results. Besides that, the very low orbital eccentricities of PSRs J1910+0423 and J1923+2022 make finding a phase-connected timing solution much more difficult, as timing software may terminate due to $e < 0$.

To address this issue, we developed a modified timing model implemented in TEMPO2 (G. B. Hobbs et al. 2006), ELL1R, in which the parameters $T_{\rm asc}$, ϵ_1, and ϵ_2 are converted back into T_0, e, and ω as follows:

$$\begin{aligned} T_0 &= T_{\rm asc} + \frac{\arctan(\epsilon_1/\epsilon_2)}{2\pi}P_{\rm orb},\\ e &= \sqrt{\epsilon_1^2+\epsilon_2^2},\\ \omega &= \arctan(\epsilon_1/\epsilon_2). \end{aligned} \quad (2)$$

The Römer delay is then computed according to the BT and DD models (R. Blandford & S. A. Teukolsky 1976; T. Damour & N. Deruelle 1985, 1986):

$$\Delta_{\rm RB} = x\sin\omega(\cos u - e) + x\sqrt{1-e^2}\cos\omega\sin u, \quad (3)$$

where u is the eccentric anomaly. This original-sense recovered model, dubbed the ELL1R model, can be applied to most systems with $e \ll 1$—including those in wide orbits with mild eccentricities of $0.01 \lesssim e \lesssim 0.1$ for which the ELL1 + model is not suitable—and avoids the strong correlation between T_0 and ω in the BT or DD model.

In the ELL1 model (C. Lange et al. 2001), the Shapiro delay $\Delta_{\rm SB}$ is approximated as

$$\Delta_{\rm SB} \approx -\frac{2Gm_{\rm c}}{c^3}\ln(1 - \sin i\sin\Phi), \quad (4)$$

where G is the gravitational constant, $m_{\rm c}$ is the companion mass, and i is the orbital inclination. Following the DD model (T. Damour & N. Deruelle 1986), we strictly compute the Shapiro delay in the ELL1R model:

$$\begin{aligned} \Delta_{\rm SB} = -\frac{2Gm_{\rm c}}{c^3}\ln\{1 - \sin i[\sin\omega(\cos u - e)\\ + \sqrt{1-e^2}\cos\omega\sin u] - e\cos u\}. \end{aligned} \quad (5)$$

Currently, aside from the Römer delay and the Shapiro delay, following the origin ELL1 model (C. Lange et al. 2001), the ELL1R model only accounts for secular variations in the orbital parameters. Consequently, for compact binary pulsars with mild eccentricities such as the double pulsar system PSR J0737−3039 A and B (A. G. Lyne et al. 2004), the DD model is still required to accurately describe the relativistic effects (T. Damour & N. Deruelle 1985, 1986).

In estimating parameter uncertainties, TEMPO2 (G. B. Hobbs et al. 2006) computes the covariance matrix C from the first-order partial derivatives. Using Equation (2), we transform the partial derivatives with respect to T_0, ω, and e into those with respect to $T_{\rm asc}$, ϵ_1, and ϵ_2. The correlation coefficient r between fitted parameter 1 and fitted parameter 2 is then given by $r = C_{12}/\sqrt{C_{11}C_{22}}$. Even for a mildly eccentric system such as PSR J1851–0108, the DD model (T. Damour & N. Deruelle 1985, 1986) yields a correlation coefficient between ω and T_0 as high as 0.998. In contrast, the ELL1R model avoids such a strong parameter correlation. For PSR J1851–0108, the highest correlation coefficient among the three orbital parameters adopted in the ELL1R model—$T_{\rm asc}$, ϵ_1, and ϵ_2—is 0.366, observed between $T_{\rm asc}$ and ϵ_2. The highest correlation coefficient among all fitting parameters is −0.887, observed between $P_{\rm orb}$ and the spin frequency derivative $\dot{\nu}$. The correlation arises from limited observational coverage, an issue that is also present in the DD model.

3. Timing Results and Discussion

Using this modified timing model, we follow the methodology of P. C. C. Freire & A. Ridolfi (2018), and successfully obtained the phase-coherent timing solutions for all three pulsars. We then iterated the data processing procedures to generate improved TOAs and timing, and obtained the final timing results of PSRs J1851–0108, J1910+0423, and J1923+2022 as listed in Table 2, and timing residuals are shown in Figure 1. We searched and did not find optical and infrared counterparts of these systems in VizieR online data catalogs (F. Ochsenbein et al. 2000) and available survey images including Pan-STARRS1 and UKIDSS (K. C. Chambers et al. 2016; A. Lawrence et al. 2007), probably caused by their old ages, large distances, and extinction. We analyze the timing results of the three pulsars independently.

3.1. PSR J1851–0108

PSR J1851–0108 has a broadened pulse as discussed by W. C. Jing et al. (2025) and shown in Figure 2. It is moving around its companion with an orbital period of 228 days and

Table 2
Timing Model Parameters and Other Important Parameters for PSRs J1851–0108, J1910+0423, and J1923+2022 in the Barycentric Dynamical Time Scale at Reference Epoch MJD 60500

Parameters	J1851–0108	J1910+0423	J1923+2022
$N_{\rm TOA}$	98	82	131
$\chi^2_{\rm min}/N_{\rm free}$	0.8249	1.1775	1.2500
R.A., α (hh:mm:ss.sss; J2000 equinox)	18:51:11.390(2)	19:10:10.2275(15)	19:23:47.4763(5)
Decl., δ (dd:mm:ss.ss; J2000 equinox)	−01: 08: 10.04(8)	+04: 23: 01.19(3)	+20: 22: 50.676(11)
Spin period, P (s)	0.08707461410585(12)	0.0932414759973(5)	0.037992888786748(15)
Spin period derivative, $\dot{P}$ (s s^{-1})	$2.75(10) \times 10^{-19}$	$9.2(5) \times 10^{-19}$	$1.812(2) \times 10^{-19}$
Spin frequency, ν (Hz)	11.484403465565(16)	10.72484094985(5)	26.320715058361(10)
Spin frequency derivative, $\dot{\nu}$ (s^{-2})	$-3.63(13) \times 10^{-17}$	$-1.06(5) \times 10^{-16}$	$-1.2552(14) \times 10^{-16}$
Characteristic age, $\tau_{\rm c}$ (Gyr)	5.0	1.6	3.3
Surface magnetic field strength, $B_{\rm s}$ (G)	5.0×10^9	9.4×10^9	2.7×10^9
Dispersion measure (pc cm^{-3})	670.96(5)	339.840(5)	175.310(6)
Dispersion measure derivative (pc cm^{-3} yr^{-1})	⋯	0.016(4)	0.007(4)
Distance from NE2001 and YMW16 (kpc)	8.8 and 6.1	8.4 and 13.1	6.2 and 4.6
Rotation measure (rad m^{-2})	319(2)	634(2)	223(4)
Binary model		**DD**	
Orbital period, $P_{\rm orb}$ (days)	228.021994(9)	885.8686(4)	777.470128(8)
Projected semimajor axis, x (lt-s)	207.92211(5)	203.3159(2)	244.613429(15)
Time of periastron passage, T_0 (MJD)	60267.67630(12)	61243.94(3)	60493.53(3)
Longitude of periastron, ω (deg)	142.23572(19)	253.885(11)	118.480(13)
Orbital eccentricity, e	0.1331659(4)	0.0026133(8)	0.00067731(18)
Weight rms of timing residuals, $\sigma_{\rm res}$ (μs)	203.142	22.582	34.540
Binary model		**ELL1+**	
Orbital period, $P_{\rm orb}$ (days)	⋯	885.8686(4)	777.470128(8)
Projected semimajor axis, x (lt-s)	⋯	203.3159(2)	244.613429(15)
Time of ascending node passage, $T_{\rm asc}$ (MJD)	⋯	60619.19547(12)	60237.658307(9)
First Laplace parameter, $\epsilon_1 \equiv e \sin\omega$	⋯	−0.0025106(8)	0.00059534(15)
Second Laplace parameter, $\epsilon_2 \equiv e \cos\omega$	⋯	−0.0007254(5)	−0.00032298(19)
Weighted rms of timing residuals, $\sigma_{\rm res}$ (μs)	⋯	22.582	34.541
Binary model		**ELL1R**	
Orbital period, $P_{\rm orb}$ (days)	228.021994(9)	885.8686(4)	777.470128(8)
Projected semimajor axis, x (lt-s)	207.92211(5)	203.3159(2)	244.613429(15)
Time of ascending node passage, $T_{\rm asc}$ (MJD)	60177.584981(9)	60619.19546(12)	60237.658309(9)
First Laplace parameter, $\epsilon_1 \equiv e \sin\omega$	0.0815527(3)	−0.0025106(8)	0.00059534(15)
Second Laplace parameter, $\epsilon_2 \equiv e \cos\omega$	−0.1052726(5)	−0.0007254(5)	−0.00032298(19)
Weight rms of timing residuals, $\sigma_{\rm res}$ (μs)	203.142	22.582	34.540
Binary model	**Derived binary parameters from ELL1R model**		
Time of periastron passage, T_0 (MJD)	60267.67630(11)	61243.94(3)	60493.53(3)
Longitude of periastron, ω (deg)	142.23572(17)	253.885(12)	118.480(15)
Orbital eccentricity, e	0.1331659(4)	0.0026133(8)	0.00067731(16)
Mass function ($M_\odot$)	0.18562277(14)	0.01149896(2)	0.025998973(4)
Minimum companion mass ($M_\odot$)	1.03	0.32	0.45

Note. Distances are estimated using the NE2001 (J. M. Cordes & T. J. W. Lazio 2002) and YMW16 (J. M. Yao et al. 2017) electron-density models. The solar system ephemeris used in this work is DE440 (R. S. Park et al. 2021).

has a mild orbital eccentricity of 0.133. The mass function $f(m_{\rm p}, m_{\rm c}, \sin i)$ of PSR J1851–0108 gives a constraint on the companion mass of

$$f(m_{\rm p}, m_{\rm c}, \sin i) = \frac{m_{\rm c}^3 \sin^3 i}{(m_{\rm p}+m_{\rm c})^2} = \frac{4\pi^2}{G}\frac{x^3}{P_{\rm orb}^2} = 0.18562277(14)\, M_\odot, \quad (6)$$

where $m_{\rm p}$ is the pulsar mass. Assuming a typical pulsar mass of 1.4 $M_\odot$, the companion mass must be greater than 1.03 $M_\odot$.

The nature of its massive companion can be as follows.

1. *A massive white dwarf companion.* In this case, probably the system has experienced stable Roche-lobe overflow instead of common envelope evolution during the mass transfer from the companion to the neutron star (H. Ge et al. 2023), and its mildly eccentric orbit may be induced by the shell flashes when producing its massive white dwarf companion (T. M. Tauris & E. P. J. van den Heuvel 2023).
2. *A main-sequence star companion.* PSR J1851–0108 is a mildly recycled pulsar with a spin period of 87.1 ms and

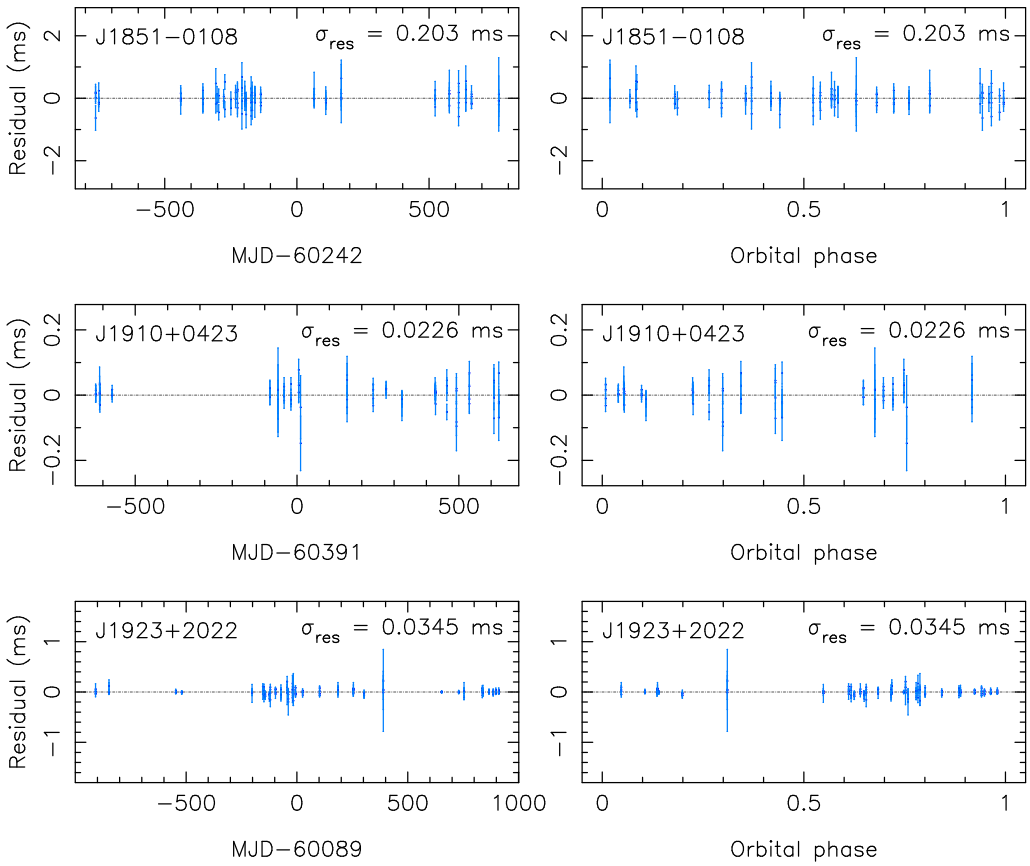


Figure 1. Timing residuals of PSRs J1851–0108, J1910+0423, and J1923+2022 as as a function of epoch or orbital phase. The error bars show the 1σ uncertainties of the measured TOAs taken with the *L*-band 19-beam receiver of FAST. No systematic trends are visible. Their weighted rms of the timing residuals $\sigma_{\rm res}$ are shown in each subpanel.

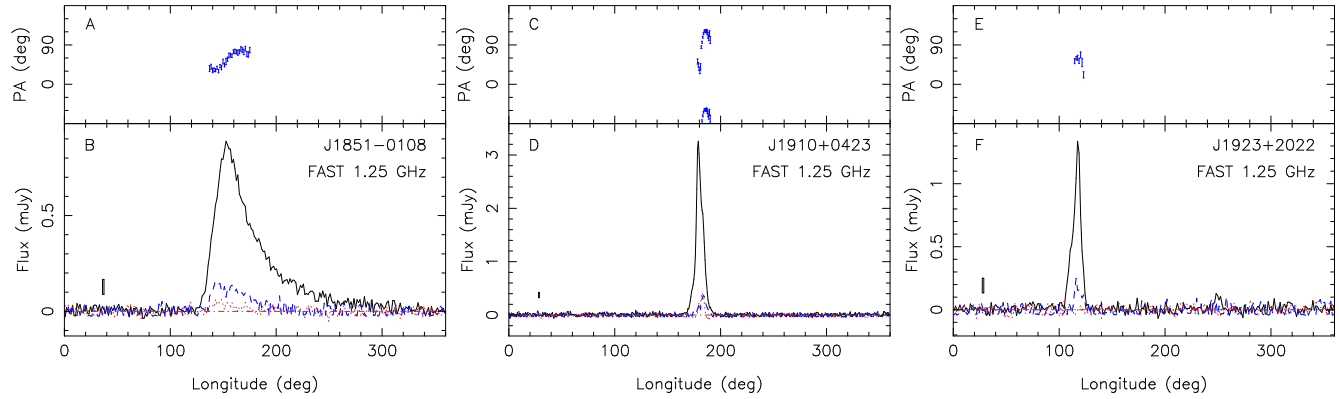


Figure 2. The polarization profiles of PSRs J1851–0108, J1910+0423, and J1923+2022 obtained by adding data from all available FAST tracking observations with a beam offset of less than 1.0′ from the pulsar position, with integration times of 2.3, 1.4, and 0.4 hr, respectively. The total intensity profile (black line), linear (blue dashed line), and circular (red dotted line, positive for the left-hand sense) polarization profiles are plotted in the lower subpanel, with a scale box indicating the 1 bin width and the $\pm2\sigma$ of the flux density. The linear polarization angles (PAs) are plotted in the upper subpanel with the error bars representing $\pm1\sigma$.

a surface magnetic field strength of 5.0×10^9 G, suggesting that this binary pulsar has accreted mass from its companion. Conventional binary stellar evolution models predict neither significant orbital eccentricities nor main-sequence companions in such a wide orbit around a recycled pulsar. However, D. J. Champion et al. (2008) have found an exception, PSR J1903+0327, to this prediction, which may be formed in a hierarchical triple system or a globular cluster.

3. *A neutron star or black hole companion.* In this case, the orbital eccentricity of PSR J1851–0108 should originate from the birth kick of its companion star. However, many studies found that a wide double neutron star system with a small orbital eccentricity is less likely to be formed (T. M. Tauris et al. 2017; Y.-L. Guo et al. 2024; Z. Chen et al. 2025). The birth kicks of black holes are still unclear (S. Repetto et al. 2012; I. Mandel 2016; T. M. Tauris & E. P. J. van den Heuvel 2023), but assuming a pulsar mass

of 1.4 $M_\odot$, the possibility that the companion mass PSR J1851–0108 is greater than 3.0 $M_\odot$ is only 14%.

3.2. PSR J1910+0423

PSR J1910+0423 has only one main pulse (see Figure 2). Our timing result shows that PSR J1910+0423 has a spin period of 93.2 ms and a surface magnetic field strength of 9.5×10^9 G, indicating that it has been mildly recycled. PSR J1910+0423 and a $\geqslant 0.32\,M_\odot$ companion are moving around each other in a 886 day orbit with an orbital eccentricity of 0.0026, therefore this binary system most likely evolved from a low-mass X-ray binary, and the companion star is either a helium white dwarf or a carbon–oxygen white dwarf (P. F. Wang et al. 2025).

E. S. Phinney (1992) predicted that such a binary pulsar should follow a relationship between its orbital period and orbital eccentricity:

$$\langle e^2 \rangle^{1/2} \approx 1.5 \times 10^{-4} (P_{\rm orb}/100\ {\rm days}). \quad (7)$$

The orbital eccentricity of PSR J1910+0423 is 0.0026, close to the expected value of 0.0013.

3.3. PSR J1923+2022

PSR J1923+2022 has a main pulse and a discrete secondary pulse with a large rotation longitude separation of about 140°. It is also a mildly recycled pulsar that has a spin period of 38.0 ms and a surface magnetic field strength of 2.7×10^9 G. Its orbital period is 777 days, and the minimum companion mass is 0.45 $M_\odot$. Similar to PSR J1910+0423, this binary pulsar is also a descendant of low-mass X-ray binaries (P. F. Wang et al. 2025). Its orbital eccentricity of 6.8×10^{-4} is consistent with the expectation of E. S. Phinney (1992) as well. The mass function of PSR J1923+2022 is larger than that of PSR J1910+0423, so this binary system should have a larger orbital inclination. T. M. Tauris & G. J. Savonije (1999) provide a relationship between the orbital period and the mass of the white dwarf companion:

$$\frac{m_{\rm c}}{M_\odot} = \left(\frac{P_{\rm orb}}{1.1 \times 10^5\ {\rm days}} \right)^{1/4.75} + 0.115. \quad (8)$$

So the expected companion mass of PSR J1923+2022 is 0.47 $M_\odot$. Compared to the minimum companion mass of 0.45 $M_\odot$, its orbit is likely close to edge on.

4. Summary and Discussion

We report FAST observations and a timing analysis of three binary pulsars—PSRs J1851–0108, J1910+0423, and J1923+2022—discovered in the FAST GPPS survey (J. L. Han et al. 2021, 2025). These systems exhibit small orbital eccentricities ($e \ll 1$) and long orbital periods of 228, 886, and 777 days, respectively (see Figure 3). We developed a modified timing model, designated as ELL1R, based on the ELL1 framework (C. Lange et al. 2001). The ELL1R model combines the strengths of both the DD (T. Damour & N. Deruelle 1985, 1986) and ELL1 (C. Lange et al. 2001) timing models. Using ELL1R, we obtained phase-connected timing solutions for all three pulsars. The timing results indicate that these objects are mildly recycled and likely accreted mass from their companions in the past. While the nature of the companion to PSR J1851–0108 remains uncertain, binary evolution models suggest that PSRs J1910+0423 and J1923+2022 have white dwarf companions and descended from low-mass X-ray binaries. In addition, PSR J1923+2022 is likely in a nearly edge-on orbit.

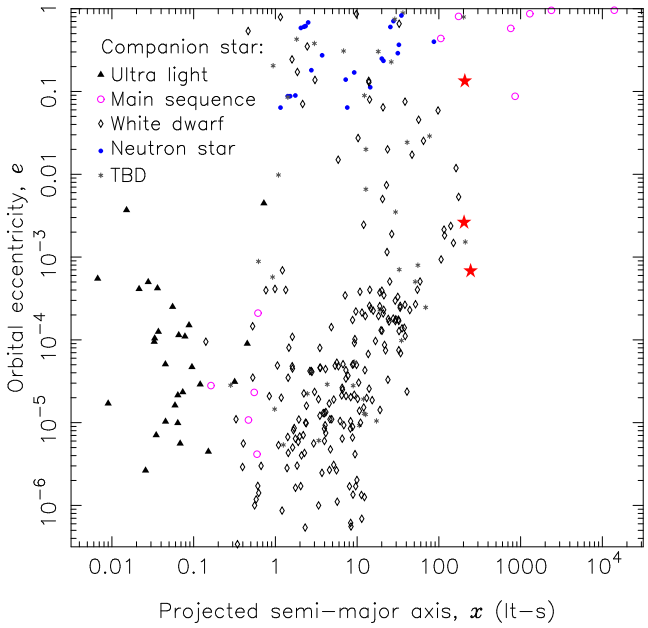


Figure 3. The distribution of projected semimajor axis x and orbital eccentricity e for binary pulsars. Data from the ATNF pulsar catalog v.2.7.0 (R. N. Manchester et al. 2005) are shown, with the three GPPS binary pulsars presented in this work highlighted as red stars.

Its application to the three pulsars demonstrates that (1) compared to the DD model, ELL1R yields consistent orbital parameters and timing residuals while significantly reducing parameter covariances, and (2) compared to the ELL1+ model, ELL1R is applicable to a broader range of binary systems and does not require the constraint $xe^4 \lesssim \sigma_{\rm TOA}/N_{\rm TOA}^{1/2}$.

To validate our modified ELL1R timing model, we compared its performance against the DD model (T. Damour & N. Deruelle 1985, 1986) in TEMPO2 (G. B. Hobbs et al. 2006) and the ELL1+ model (W. W. Zhu et al. 2019; W. Fiore et al. 2023) in PINT (J. Luo et al. 2021).

For PSRs J1910+0423 and J1923+2022, the condition $xe^4 \lesssim \sigma_{\rm TOA}/N_{\rm TOA}^{1/2}$ is satisfied, indicating that the low-eccentricity approximation used in ELL1+ remains valid. In these cases, the ELL1R model produces timing solutions and residuals consistent with those from ELL1+. In contrast, for PSR J1851–0108, where xe^4 reaches 0.065 lt-s, the low-eccentricity approximation breaks down, rendering the ELL1+ model inapplicable. Notably, for all three pulsars, the timing residuals obtained with the ELL1R and DD models are identical.

However, the DD model exhibits strong covariances between T_0 and ω, leading to significantly larger uncertainties in T_0 compared to $T_{\rm asc}$ (see Table 2). This complicates the accurate reproduction of timing results using the reported DD parameters unless more significant digits are retained.

As shown in Equation (2), the DD parameters T_0, e, and ω can be derived from $T_{\rm asc}$, ϵ_1, and ϵ_2. Under the assumption of independent errors among $T_{\rm asc}$, ϵ_1, and ϵ_2, the uncertainties of T_0, e, and ω can be estimated via the law of propagation of uncertainties. Using this method, we confirmed that the orbital

parameters derived from the ELL1R model are consistent with those obtained from the DD model.

Acknowledgments

This work made use of the data from FAST.[7] FAST is a Chinese national megascience facility, operated by National Astronomical Observatories, Chinese Academy of Sciences. The authors were supported by the National Natural Science Foundation of China (NSFC), grant Nos. 12588202 and 12041303, National Key R&D Program of China No. 2025YFA161400, the Chinese Academy of Sciences via project JZHKYPT-2021-06, and the National SKA Program of China grant 2020SKA0120100 and 2022SKA0120103.

Facility: FAST.

Software: PINT (J. Luo et al. 2021), TEMPO2 (G. B. Hobbs et al. 2006), PSRCHIVE (A. W. Hotan et al. 2004), DSPSR (W. van Straten & M. Bailes 2011), PRESTO (S. M. Ransom 2001).

ORCID iDs

Z. L. Yang https://orcid.org/0009-0009-6590-1540
J. L. Han https://orcid.org/0000-0002-9274-3092
W. Q. Su https://orcid.org/0009-0003-2212-4792
C. Wang https://orcid.org/0009-0004-3433-2027
J. P. Yuan https://orcid.org/0000-0002-5381-6498
T. Wang https://orcid.org/0000-0002-4704-5340
Yi Yan https://orcid.org/0009-0008-1612-9948
J. Xu https://orcid.org/0000-0003-1778-5580
W. C. Jing https://orcid.org/0000-0002-1056-5895
P. F. Wang https://orcid.org/0000-0002-6437-0487
N. N. Cai https://orcid.org/0000-0002-5915-5539
D. J. Zhou https://orcid.org/0000-0002-6423-6106
D. Zhao https://orcid.org/0009-0007-8062-1454

References

Bhattacharyya, B., & Nityananda, R. 2008, MNRAS, 387, 273
Blandford, R., & Teukolsky, S. A. 1976, ApJ, 205, 580
Chambers, K. C., Magnier, E. A., Metcalfe, N., et al. 2016, arXiv:1612.05560
Champion, D. J., Ransom, S. M., Lazarus, P., et al. 2008, Sci, 320, 1309
Chen, X., Han, J. L., Su, W. Q., Yang, Z. L., & Zhou, D. J. 2023, RAA, 23, 104004
Chen, Z., Zhang, J., Lu, Y., Liu, J., & Zeng, C. 2025, MNRAS, 544, L89
Cordes, J. M., & Lazio, T. J. W. 2002, arXiv:astro-ph/0207156
Damour, T., & Deruelle, N. 1985, AIHPA, 43, 107
Damour, T., & Deruelle, N. 1986, AIHPA, 44, 263
Damour, T., & Schaefer, G. 1991, PhRvL, 66, 2549
Fiore, W., Levin, L., McLaughlin, M. A., et al. 2023, ApJ, 956, 40
Freire, P. C. C., & Ridolfi, A. 2018, MNRAS, 476, 4794
Ge, H., Tout, C. A., Chen, X., et al. 2023, ApJ, 945, 7
Guo, Y.-L., Wang, B., Chen, W.-C., et al. 2024, MNRAS, 530, 4461
Han, J. L., Wang, C., Wang, P. F., et al. 2021, RAA, 21, 107
Han, J. L., Zhou, D. J., Wang, C., et al. 2025, RAA, 25, 014001
Hobbs, G. B., Edwards, R. T., & Manchester, R. N. 2006, MNRAS, 369, 655
Hotan, A. W., van Straten, W., & Manchester, R. N. 2004, PASA, 21, 302
Hulse, R. A., & Taylor, J. H. 1975, ApJL, 195, L51
Jing, W. C., Han, J. L., Wang, C., et al. 2025, arXiv:2506.14519
Lange, C., Camilo, F., Wex, N., et al. 2001, MNRAS, 326, 274
Lawrence, A., Warren, S. J., Almaini, O., et al. 2007, MNRAS, 379, 1599
Luo, J., Ransom, S., Demorest, P., et al. 2021, ApJ, 911, 45
Lyne, A. G., Burgay, M., Kramer, M., et al. 2004, Sci, 303, 1153
Manchester, R. N., Hobbs, G. B., Teoh, A., & Hobbs, M. 2005, AJ, 129, 1993
Mandel, I. 2016, MNRAS, 456, 578
Nan, R. 2006, ScChG, 49, 129
Nice, D., Demorest, P., Stairs, I., et al. 2015, Tempo: Pulsar timing data analysis Astrophysics Source Code Library, ascl:1509.002
Ochsenbein, F., Bauer, P., & Marcout, J. 2000, A&AS, 143, 23
Park, R. S., Folkner, W. M., Williams, J. G., & Boggs, D. H. 2021, AJ, 161, 105
Phinney, E. S. 1992, RSPTA, 341, 39
Ransom, S. M. 2001, PhD thesis, Harvard Univ.
Repetto, S., Davies, M. B., & Sigurdsson, S. 2012, MNRAS, 425, 2799
Susobhanan, A., Gopakumar, A., Joshi, B. C., & Kumar, R. 2018, MNRAS, 480, 5260
Tauris, T. M., & Savonije, G. J. 1999, A&A, 350, 928
Tauris, T. M., & van den Heuvel, E. P. J. 2023, Princeton Series in Astrophysics, Vol. 68, Physics of Binary Star Evolution: From Stars to X-ray Binaries and Gravitational Wave Sources (Princeton Univ. Press)
Tauris, T. M., Kramer, M., Freire, P. C. C., et al. 2017, ApJ, 846, 170
van Straten, W., & Bailes, M. 2011, PASA, 28, 1
Wang, P. F., Han, J. L., Xu, J., et al. 2023, RAA, 23, 104002
Wang, P. F., Han, J. L., Yang, Z. L., et al. 2025, RAA, 25, 014003
Wex, N. 1997, A&A, 317, 976
Wex, N. 2000, ASPC, 202, 113
Will, C. M. 1993, Theory and Experiment in Gravitational Physics (Cambridge Univ. Press)
Yang, Z. L. 2025, Zony-naoc/ELL1Rmodel: A modified version of the ELL1 model in TEMPO2, Version Pulsar_timing , Zenodo, doi:10.5281/zenodo.18050544
Yao, J. M., Manchester, R. N., & Wang, N. 2017, ApJ, 835, 29
Zhu, W. W., Desvignes, G., Wex, N., et al. 2019, MNRAS, 482, 3249

[7] https://cstr.cn/31116.02.FAST